Supporting Information: Manipulating Topological Domain Boundaries in the Single-Layer Quantum Spin Hall Insulator 1T'–WSe_2

Zahra Pedramrazi[1†], Charlotte Herbig[1†], Artem Pulkin[2,3†], Shujie Tang[4,5,6], Madeleine Phillips[7,8], Dillon Wong[1], Hyejin Ryu[4,9], Michele Pizzochero[2], Yi Chen[1], Feng Wang[1,10,11], Eugene J. Mele[7], Zhi-Xun Shen[5,6], Sung-Kwan Mo[4], Oleg V. Yazyev[2,12], Michael F. Crommie[1,10,11*]

[1]Department of Physics, University of California at Berkeley, Berkeley, CA 94720, USA.

[2]Institute of Physics, Ecole Polytechnique Fédérale de Lausanne (EPFL), CH-1015 Lausanne, Switzerland.

[3]Division of Chemistry and Chemical Engineering, California Institute of Technology, Pasadena, CA 91125, USA.

[4]Advanced Light Source, Lawrence Berkeley National Laboratory, Berkeley, CA 94720, USA.

[5]Stanford Institute for Materials and Energy Sciences, SLAC National Accelerator Laboratory, Menlo Park, CA 94025, USA.

[6]Geballe Laboratory for Advanced Materials, Departments of Physics and Applied Physics, Stanford University, Stanford, CA 94305, USA.

[7]Department of Physics and Astronomy, University of Pennsylvania, Philadelphia, PA 19104, USA.

[8]Center for Computational Materials Science, Naval Research Laboratory, Washington, D.C. 20375, USA.

[9]Center for Spintronics, Korea Institute of Science and Technology, Seoul 02792, Korea.

[10]Materials Sciences Division, Lawrence Berkeley National Laboratory, Berkeley, CA 94720, USA.

[11]Kavli Energy NanoScience Institute at the University of California Berkeley and the Lawrence Berkeley National Laboratory, Berkeley, CA 94720, USA.

[12]National Centre for Computational Design and Discovery of Novel Materials MARVEL, Ecole Polytechnique Fédérale de Lausanne (EPFL), CH-1015 Lausanne, Switzerland.

† These authors contributed equally to this work.

*e-mail: crommie@berkeley.edu

1- Position-dependent STS near a 0° domain boundary

The 120° domain boundary is the most commonly observed line defect (85% of observed domain boundaries). The 0° domain boundary is the second most common type of induced 1T'/1T' domain boundary (13% of observed domain boundaries). The 60° domain boundary is the least common type (2% of observed domain boundaries). Detailed position-dependent spectroscopic measurements show that the signature of the bulk gap is always observed in STS of 0° domain boundaries (Fig. S1).

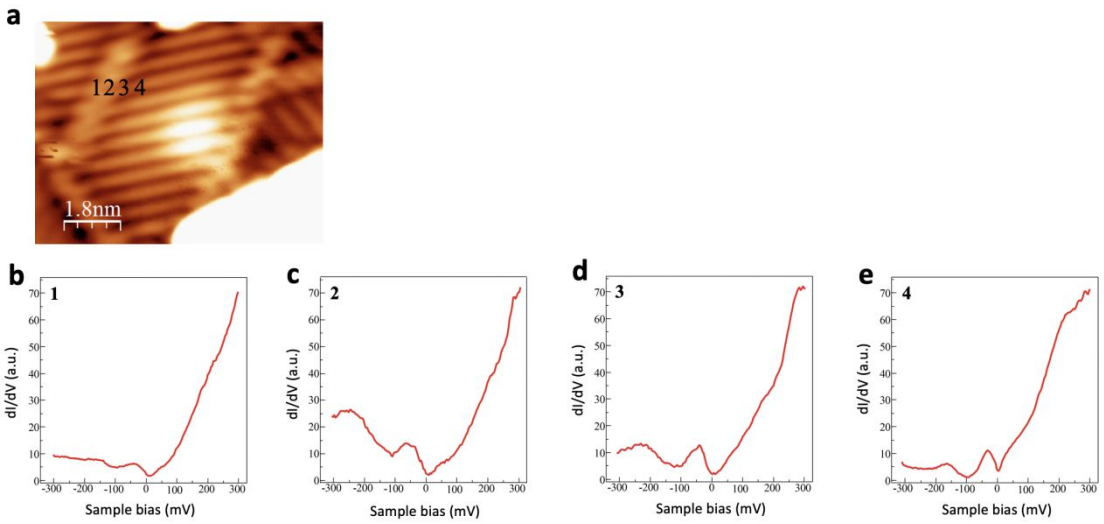

Figure S1: Position-dependent STS of 0° 1T'/1T' domain boundary in single layer 1T'–WSe_2. (a) STM image of 1T'–WSe_2 with 0° domain boundary (standard STM topograph). (b)-(d) dI/dV spectra obtained at locations on and near 0° domain boundary as marked in (a) (initial tunneling parameters: f = 613.7 Hz, V_{ac} = 4 mV, I = 100 pA, V_s = –400 mV, T = 4.5 K).

2- Position-dependent STS near 120° domain boundary

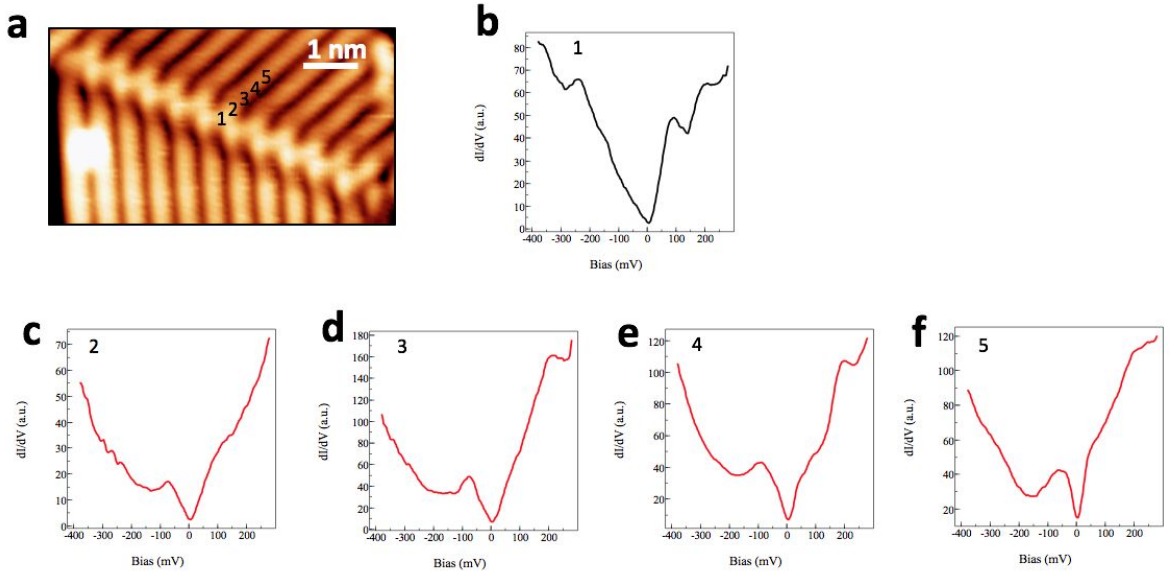

Figure S2: Position-dependent STS of 120° domain boundary in 1T'–WSe_2. (a) STM image of 1T'–WSe_2 with 120° domain boundary (standard STM topograph). (b)-(f) dI/dV spectra obtained at locations on and near 120° domain boundary as marked in (a) (Initial tunneling parameters: f = 613.7 Hz, V_{ac} = 4 mV, I = 100 pA, V_s = –400 mV, T = 4.5 K).

3- Simulated domain-boundary structures

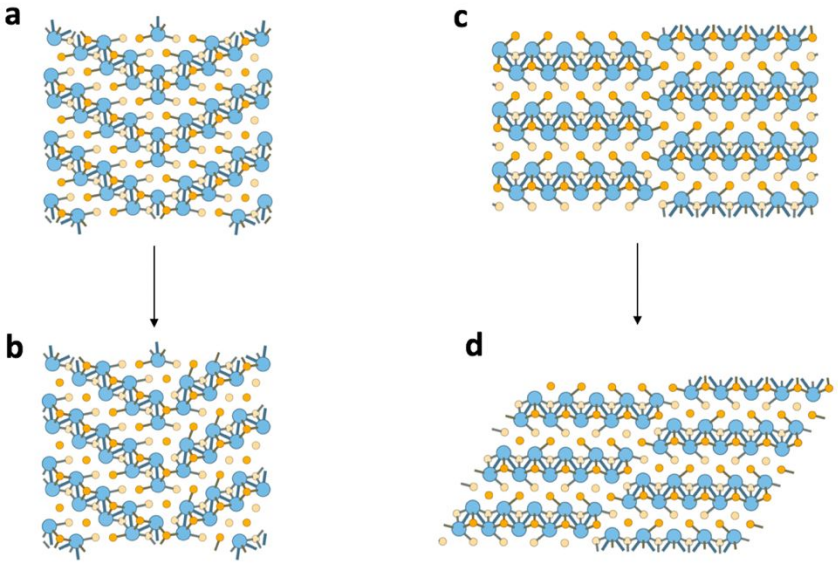

Figure S3: Structures and breaking of the symmetry of domain-boundary structures. (a) Symmetric 120° domain boundary with a mirror symmetry. (b) Non-symmetric 120° domain-boundary structure. The energy is reduced by 32 meV/Å relative to the structure in (a). (c,d) 0° domain boundaries with different orientations. The structure in (d) is lower in energy by 15 mV/Å compared to the structure in (c).

4- 1T'–vacuum termination vs. 1T'/1T' domain boundaries

A representative illustration of the different possible interface state electronic behaviors (trivial versus non-trivial) is given in Figs. S4a,b. Here the ballistic flow of charge carriers having different spin polarization is indicated. Fig. S4b shows how charge carriers with either spin polarization traveling along the unprotected interface are able to backscatter. This is seen theoretically in DFT calculations for the 120° domain boundary states where the bulk band gap does not fully close and a non-zero energy gap of value ~ 20 mV still exists (Fig. 4a). Even though the 60° domain boundary states span the bulk gap they remain topologically unprotected (Fig. 4b).

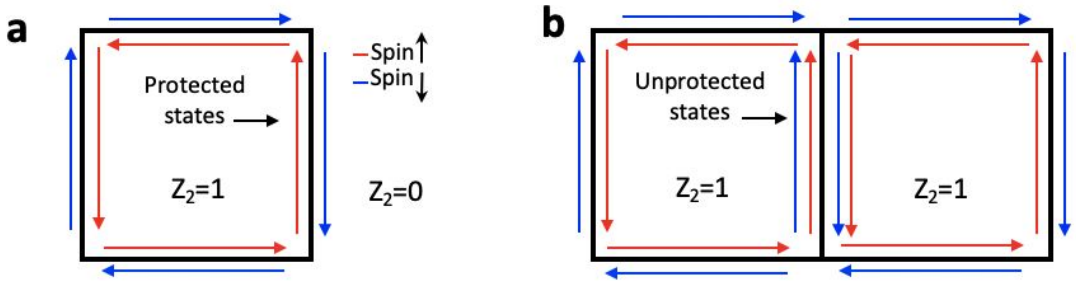

Figure S4: (a) Schematic representation of a QSHI terminated by vacuum. (b) Schematic representation of two different QSHIs fused at a single interface.

5- Electronic structure of the 1T'–vacuum termination

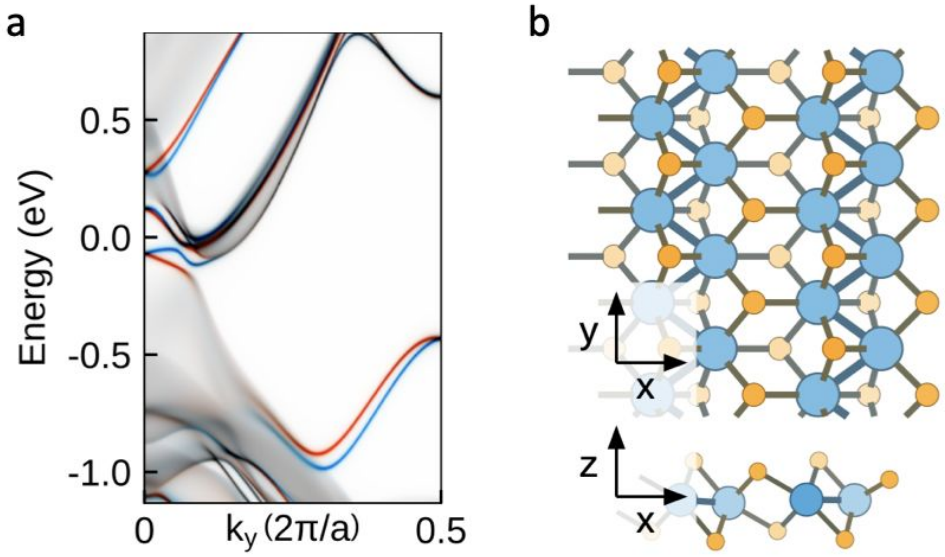

Figure S5: (a) The simulated spin-projected DOS of a vacuum-terminated edge of monolayer 1T'–WSe_2 (color = spin). The corresponding atomic structure of the model is shown in (b).

6- Analysis of tip-induced 1H domain

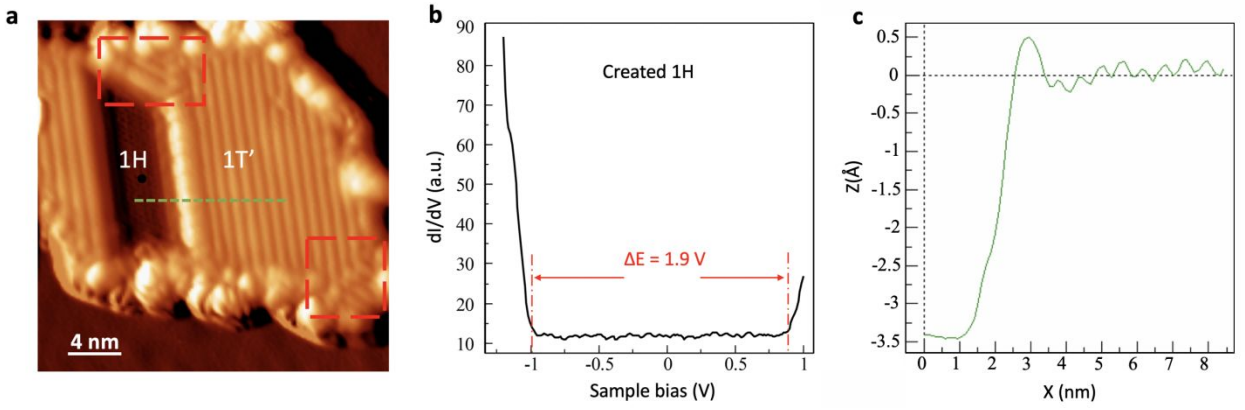

Figure S6: Measurement of tip-induced 1H domain. (a) STM image of a 1H domain created by applying a tip voltage pulse (V_{pulse} = 10 V, Δt = 100 ms, tip height ~ 6 Å) to monolayer 1T'–WSe_2. Red dashed boxes indicate small 1T'/1T' domain boundaries. (b) STM dI/dV spectroscopy measured at the black circle reflects the semiconducting nature of the 1H domain.

(Initial tunneling parameters: f = 613.7 Hz, V_{ac} = 40 mV, I = 100 pA, V_s = –1.3 eV, T = 4.5 K, image intensity proportional to dz/dx where z is STM tip height). (c) line-profile taken at the green dashed line, shows height difference of 3.43 Å between the 1T' and 1H structural phases. This apparent height difference reflects the difference in electronic properties between the 1H and 1T' structural phases (since the 1H phase is a topologically trivial semiconductor).

7- Evidence for ferroelasticity

Fig. S7a shows a topographic STM image after applying a 10 V tip voltage pulse on a single-domain island. Contaminants appear on the island and multiple 1T' rotated domains separated by 1T'/1T' domain boundaries are formed. Fig. S7b shows the same area after positioning the tip close to the surface and raster-scanning over the sample with relatively large tunnel current (1 nA). The contaminants on the substrate our now mostly gone and the island no longer exhibits any 1T'/1T' domain boundaries. The island is now a single, homogeneous 1T' domain with only one orientation. Similar behavior was observed numerous times in large islands, where contaminants on the surface appeared to aid in 1T'/1T' domain boundary formation and removal of the contaminants caused restoration of the original single 1T' domain. These measurements provide evidence that 1T'–WSe_2 is ferroelastic since the contaminants likely cause strain in the 1T' layer, thus explaining why their removal restores the island to its original state. Strain signatures are also present in the 1T' to 1H phase transition process. 1T'/1T' domain boundaries are observed in all islands that underwent the phase transition from 1T' to 1H (1T'/1T' domain boundaries in Fig. 1b are boxed by dashed lines in Fig. S6).

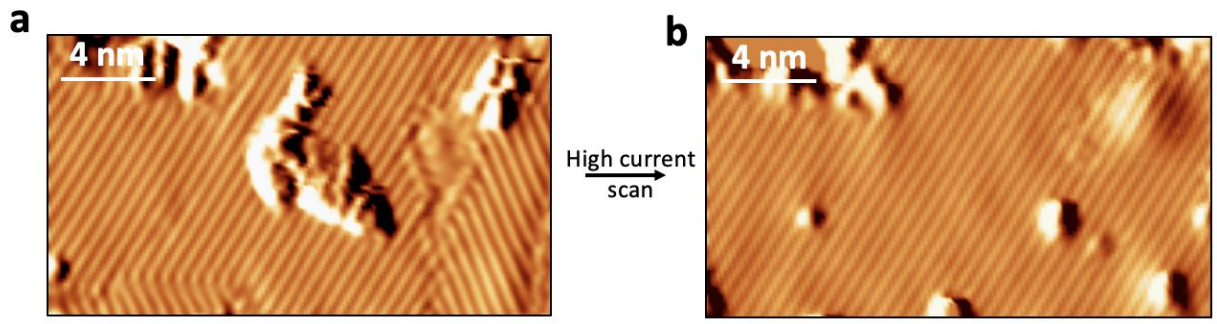

Figure S7: (a) STM image of a monolayer 1T'–WSe_2 island after applying a voltage pulse (V_{pulse} = 10 V). (b) STM topographic image of the same island imaged after scanning with high current (1 nA). (Tunneling parameters: V_s = 1V; I_t =10 pA; T = 4.5 K for all measurements, image intensity proportional to the magnitude of dz/dx where z is STM tip height.)

8- Spectroscopy measurements of topological edge state

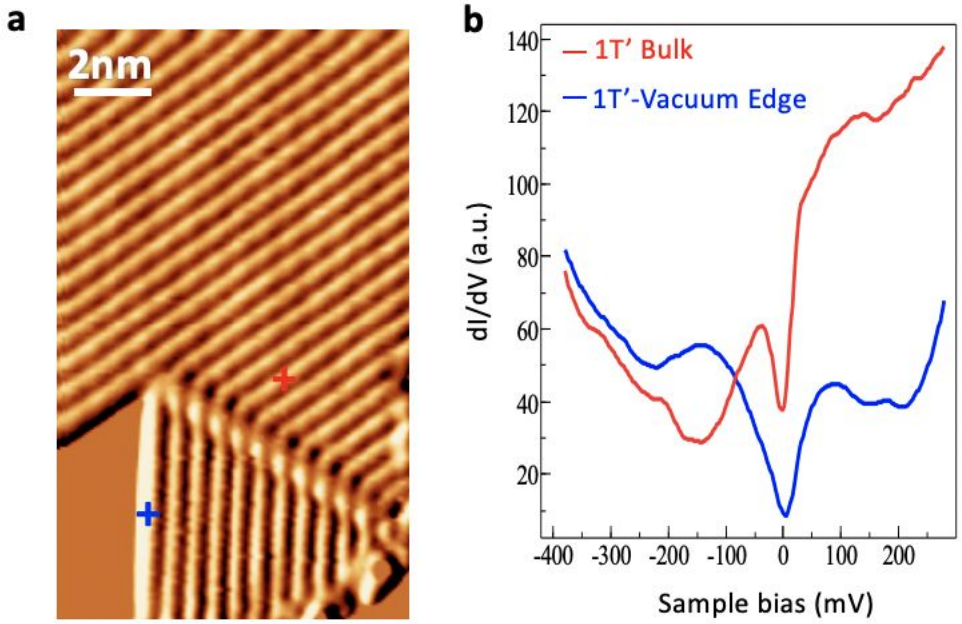

Figure S8: STS measurement of topological edge state. (a) STM image of WSe_2 island with a 120° domain boundary surrounded by vacuum-terminated edges (V_s = 1V, I_t = 10 pA, image intensity proportional to the magnitude of dz/dx where z is STM tip height). (b) dI/dV spectra measured at the 1T'–vacuum boundary (blue cross in (a)) and in the 1T'–WSe_2 bulk (red cross in

(a)). The peak centered at V = –150 mV is a signature of topologically-protected edge states. (Initial tunneling parameters: f = 613.7 Hz, V_{ac} = 4 mV, I = 100 pA, V_s = –400 mV, T = 4.5 K)

9- Detailed d*I*/d*V* maps of 120° domain boundary

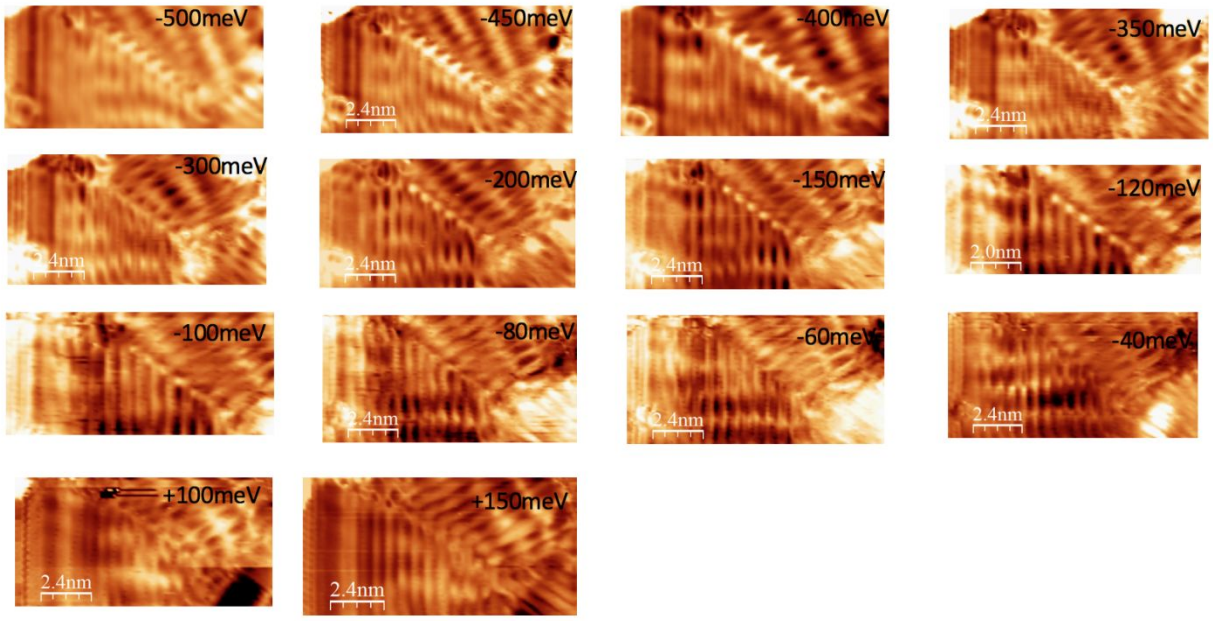

Figure S9: Constant-current d*I*/d*V* maps of mixed-phase WSe_2 island including the 120° domain boundary. The different images were acquired at different sample biases (f = 613.7 Hz, V_{ac} = 4 mV, T = 4.5 K, I = 100 pA, image intensity proportional to magnitude of dI/dV). The domain boundary state is "on" over the range –500mV < V_s < –100 mV. The QSH edge state is "on" over the range –150 mV < V_s < –60 mV.

10- Decay length analysis

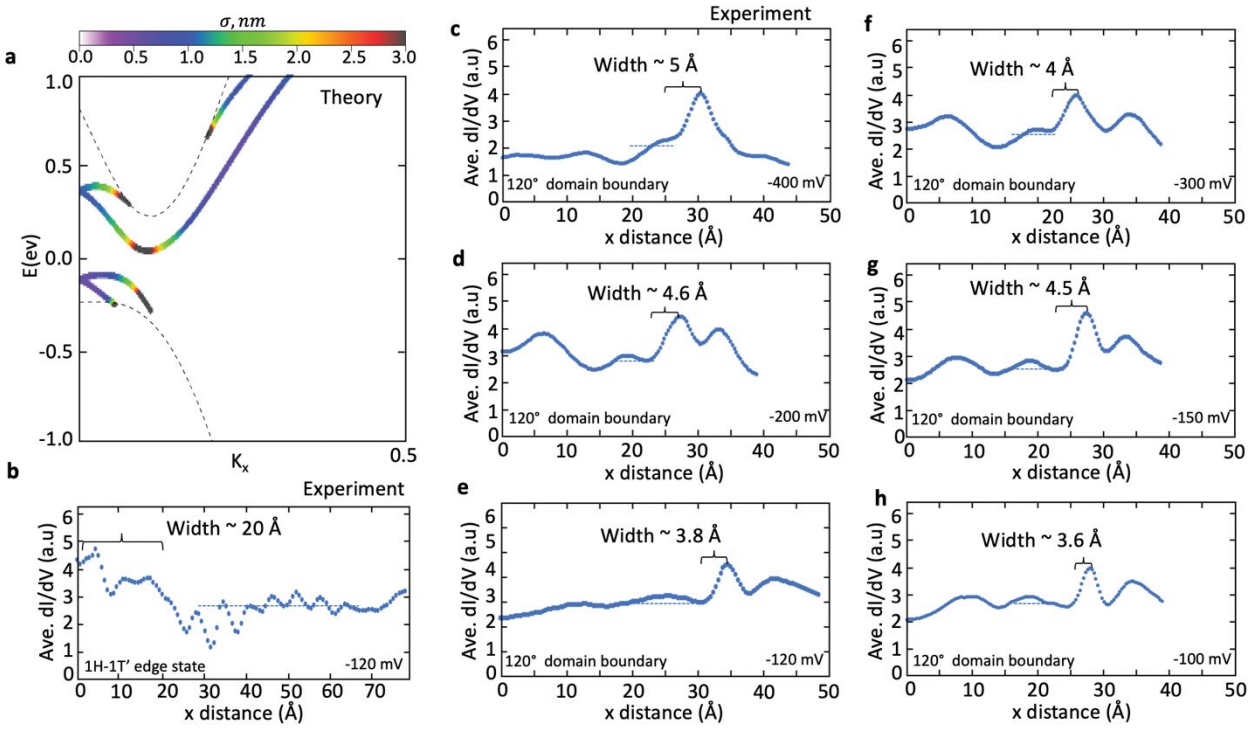

Figure S10: Theoretical and experimental analysis of the decay length for 120° domain boundary states. (a) Color-coded characteristic decay length, σ, as a function of energy, *E*, and pseudomomentum, *k*, for the 120° domain boundary. (b) 1T'/1H edge state decay length extracted from dI/dV map at energy -120mV. Decay length of 120° domain boundary extracted from dI/dV maps at (c) -400mV, (d) -200mV, (e) -120mv, (f) -300mV, (g) -150mV, and (h) -100mV.

The calculation in Fig. S10a compares the local single-particle density of states in two pairs of adjacent unit cells at both sides of the 1T'-1T' domain boundary (the average is shown)

$$\sigma(k,E) \approx a \cdot ln\frac{\rho_i(k,E)}{\rho_{i+1}(k,E)},$$

where *a* is a combination of unit cell vectors, ρ are density values (Bloch's law is assumed).

The experimental decay length was extracted from dI/dV map measurements where the dI/dV signal is averaged along the y-direction (parallel to the line defect) and plotted as a function of x (perpendicular to the line defect) in Figs. S10b-h. The decay length of the edge state at the 1T'/1H interface is measured to be 2nm. The decay length of the 120° 1T'/1T' domain boundary state is seen to be more strongly energy -dependent (~4Å at -120mV and ~6.5Å at -400mV). These experimental values are comparable to the theoretical values shown in Fig. S10a.

11- 1T`-1T` LDOS plots with different Gaussian smearing values

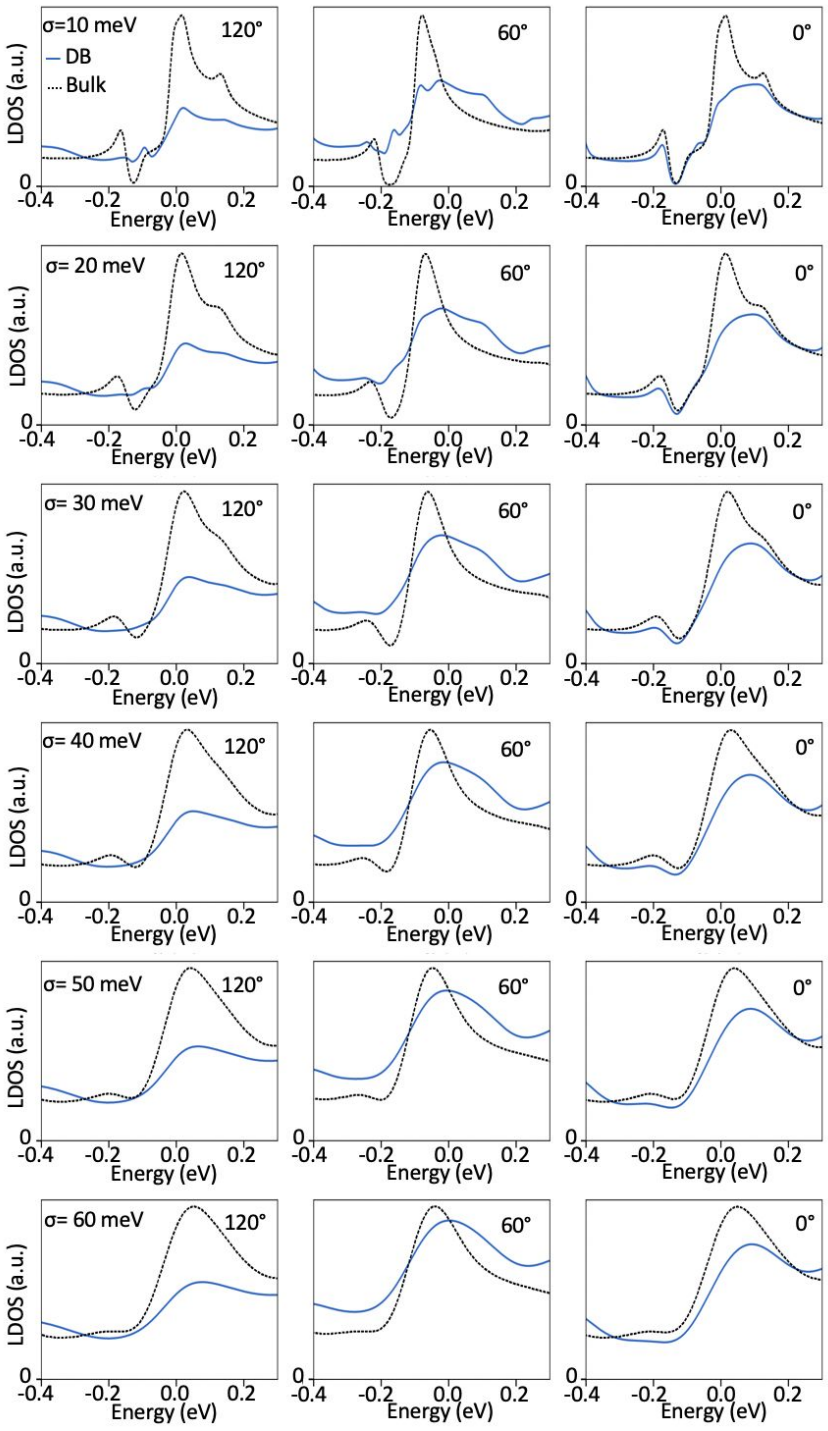

Figure S11: Simulated LDOS of the three 1T'/1T' domain boundaries plotted with different Gaussian smearing values.

12- Non-trivial and trivial two-channel system

Topologically protected edges states host counter-propagating spin states as illustrated in Figs. 4a,b of the main manuscript. Here we describe how trivial 1T'/1T' domain boundaries could potentially provide a useful conduction channel in a hypothetical two-channel device made from single-layer 1T'–WSe_2. For simplicity we will focus on only one spin direction. Following the reasoning described in Ref. 1, a trivial domain boundary channel can act as a pathway that short-circuits QSH edge states. Backscattering is allowed in the domain boundary channel but is suppressed if the boundary is sufficiently clean. QSH channels bisected by such trivial domain boundaries can be turned "on and off" by tuning the chemical potential into and out of an energy range that coincides with domain boundary states (Fig. S12). At energies near the top of the bulk gap (close to where the 120° domain boundary is expected to have a small bandgap (Figs. 3d, 4d)) the trivial channel is turned off. However, at slightly lower energies (Fig. 3c) outside the small bandgap, the 120° domain boundary hosts states and hence could reroute QSH current either fully or partially, similar to behavior predicted for graphene in the quantum Hall regime[1] (Fig. S12).

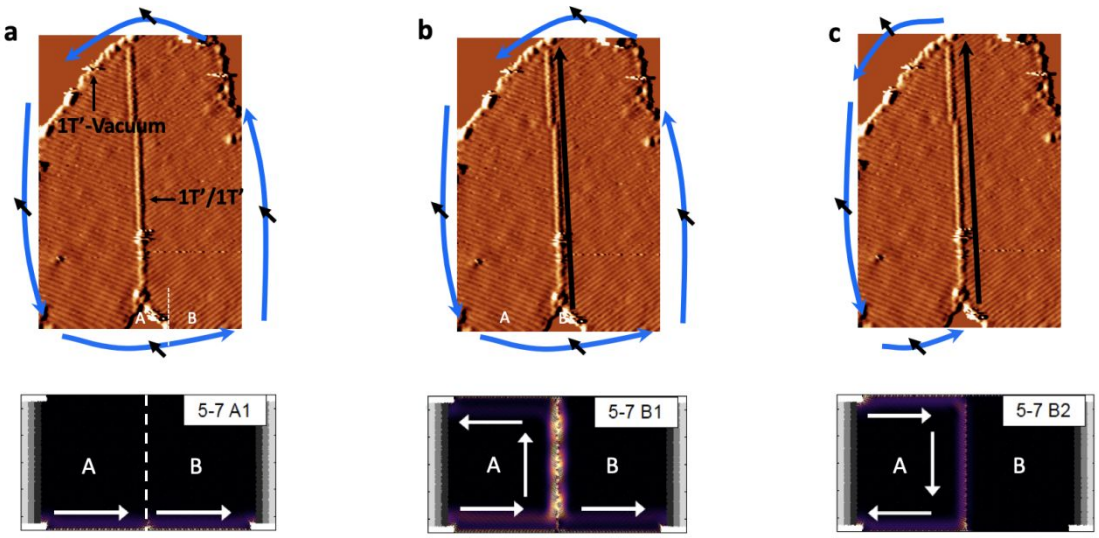

Figure S12: Trivial/topological two-channel system. (a-c) Upper images are the same STM image of a single 120° domain boundary connecting QSH edge states for 1T'–WSe_2 (V_s = 1V, I = 10 pA, T = 4.5 K, image intensity proportional to magnitude of dz/dx where z is STM tip height). Arrows are drawn to indicate the possible direction of spin-polarized current in a hypothetical device which (depending on gate voltage) could either (a) bypass the trivial domain boundary state, or (b) be rerouted partially, or (c) be rerouted fully. The lower images are model calculations of an analogous graphene device structure taken from Philips et. al.[1] Here the A and B regions are graphene domains separated by a 5-7 grain boundary located at the position of the white dashed line.

REFERENCES:

1 Phillips, M.; Mele, E. J. Charge and Spin Transport on Graphene Grain Boundaries in a Quantizing Magnetic Field. *Physical Review B* **2017**, 96, 041403.